JM PAPERS

A new wall function method for hypersonic laminar boundary layers

Fan Mo[1] and Zhenxun Gao[1],†

[1]National Laboratory for Computational Fluid Dynamics, School of Aeronautic Science and Engineering, Beihang University, Beijing 100191, PR China

A new wall function method for hypersonic laminar boundary layers (HLBLs) is proposed to reduce the near-wall grid dependence of skin friction c_f and wall heat flux q_w in numerical simulations, aiming for fast and accurate predictions. First, an analytic laminar velocity law of the wall is derived, which achieves a universal scaling of the near-wall velocity of HLBLs. Then an accurate temperature–velocity relation is deduced by introducing the general recovery factor to address the invalidation of the Walz relation under the cold wall effect. Based on the laminar laws of the wall, a new wall function method for HLBLs is proposed. To avoid introducing the boundary layer edge quantities, the laminar laws of the wall are reformed by modifying the outer boundary conditions of the differential equation in deriving the temperature–velocity relation. Unlike the wall function method in turbulence, the new wall function obtains directly the accurate c_f and q_w by post-processing without being involved in the simulation iteration. The numerical experiments of a Mach 8 HLBL over the flat plate show that effectively, the new wall function can enlarge the distance of the first grid point off the wall Δy_1 from 10^{-6} m to 10^{-3} m, which brings a 50 times enhancement of the simulation efficiency. Meanwhile, the simulation errors of c_f and q_w of the mesh with $\Delta y_1 = 10^{-3}$ m are reduced significantly from 24.2 % and 18.5 % to 0.5 % and 0.1 %, respectively. Due to the new wall function removing the boundary layer edge quantities, success is also achieved under the curved walls.

Key words: compressible boundary layers, hypersonic flow, computational methods

1. Introduction

The fast and accurate prediction of skin friction c_f and wall heat flux q_w is a critical issue in the aerodynamic/aerothermal numerical simulation of hypersonic vehicles. The velocity and temperature in hypersonic boundary layers vary sharply near the wall, which

† Email address for correspondence: gaozhenxun@buaa.edu.cn

brings great difficulties in predicting c_f and q_w accurately. Available studies (Hoffmann, Siddiqui & Chiang 2013; Thivet, Besbes & Knight 2013) have shown that simulation results for c_f and q_w are highly sensitive to the distribution of grid points near the wall, especially the distance of the first grid point off the wall Δy_1. To calculate accurately c_f and q_w of a hypersonic vehicle, Δy_1 needs to be very small, generally 10^{-6} m or even smaller, which brings a huge computational consumption. For three-dimensional complicated configurations, the numerical integration time step is limited greatly by the dense mesh, resulting in even unacceptable computational consumption.

For compressible turbulent boundary layers (CTBLs), the effective wall function method has been developed to relax the restrictions on Δy_1 in simulating c_f and q_w (Wilcox 2006), which uses the laws of the wall to represent the distribution of velocity and temperature, and obtains c_f and q_w indirectly, instead of resolving the near-wall region of CTBLs. Based on the incompressible wall function, Nichols & Nelson (2004) first introduced the compressible velocity log law (White 1991) and temperature–velocity relation (Walz 1969), then proposed a compressible wall function, which is effective uniformly in the inner layer of CTBLs and involves a compressibility effect, thus making it possible to use the wall function method to obtain c_f and q_w in CTBLs. Subsequently, Gao, Jiang & Lee (2013) revised the parameters in the laws of the wall used by Nichols according to theoretical analysis and numerical experiments, and achieved a more accurate coupling of wall function with computational fluid dynamics (CFD) codes. The simulation results of Gao *et al.* (2013) for CTBLs show that the wall function can still predict c_f and q_w accurately with $\Delta y_1^+ < 400$, which greatly improves simulation efficiency.

However, the wall function method developed above can be applied only to CTBLs. When the hypersonic vehicle flies at an altitude of more than 40 km, most of the boundary layers on the surface of the vehicle are laminar, and the wall function developed for the CTBLs will no longer be applicable. In fact, the simulation of c_f and q_w in hypersonic laminar boundary layers (HLBLs) also requires high-density grids near the wall. If there is a suitable wall function method for laminar boundary layers, then it can also effectively improve the simulation efficiency while ensuring accuracy. At present, there is no relevant research on the wall function method for HLBLs, and even whether the wall function for HLBLs can be constructed has not been explored. According to the construction method of the wall function for CTBLs, the analytic forms of the laws of the wall for HLBLs are required. For the velocity law of the wall, although self-similarity solutions exist in HLBLs at a flat plate (Anderson 2006), they cannot be used to construct the wall function due to the non-analytic form. For the temperature–velocity relation, the modified relation given by Walz based on the Crocco–Busemann relation can also be used for the compressible laminar boundary layers with a value of recovery factor different to that of CTBLs. However, it is reported that the Walz relation fails in CTBLs with cold wall boundary conditions (Duan, Beekman & Martín 2010; Duan & Martín 2011). It can be predicted that when the Walz relation is applied to the HLBLs, it will also be invalid under the strong cold wall effect. To deal with this issue, Zhang *et al.* (2014) proposed the concept of a general recovery factor to introduce the cold wall effect, and obtained a general relation between the mean velocity and temperature in CTBLs. However, the turbulent-related quantities (like effective turbulent Prandtl number) used in the Zhang *et al.* (2014) derivation cannot be defined in the laminar boundary layers, indicating that there is no theoretical basis for extending this relation directly to HLBLs. Therefore, it is necessary to conduct a derivation for HLBLs. In conclusion,

Case	Ma_∞	H (km)	p_∞ (Pa)	T_∞ (K)	Re (m^{-1})	T_w (K)	$\Theta = T_w/T_r$
M6Θ0.16	6	50	79.78	270.65	1.19×10^5	300	0.160
M8Θ0.09	8	50	79.78	270.65	1.59×10^5	300	0.093
M10Θ0.06	10	50	79.78	270.65	1.99×10^5	300	0.062

Table 1. Boundary conditions for numerical simulation.

a series of detailed works need to be carried out to develop the wall function method for HLBLs.

This paper aims to propose a new wall function method for HLBLs, so as to reduce the near-wall grid dependence of the simulation for c_f and q_w, and then achieve fast and accurate prediction. First, the near-wall velocity law of the wall and the temperature–velocity relation of HLBLs are derived theoretically and verified by numerical simulation. Then a new wall function method for HLBLs is proposed based on the laminar laws of the wall, and the numerical applications are carried out based on the typical HLBL flows. Finally, the accuracy of c_f and q_w predicted by the new wall function, as well as the efficiency improvement in numerical simulation, are analysed and discussed.

2. Laws of the wall for HLBLs

The key to constructing the wall function method is the analytic form of laws of the wall within the boundary layers, especially the accurate laws near the wall. Therefore, this section derives theoretically the temperature–velocity relation and the near-wall velocity law of the wall in HLBLs, and their accuracy is examined by numerical simulations.

2.1. *Temperature–velocity relation*

For the compressible laminar boundary layers with zero-pressure gradient, Walz (1969) used to modify the Crocco–Busemann relation by introducing the recovery factor $r \approx Pr^{0.5}$ to involve the $Pr \neq 1$ effect of air. This relation is known as the Walz relation,

$$T = T_w + (T_r - T_w)\frac{u}{u_e} + (T_e - T_r)\left(\frac{u}{u_e}\right)^2, \qquad (2.1)$$

where $T_r = T_e + ru_e^2/(2c_p)$, and subscript e means the boundary layer edge. However, previous research (Duan *et al.* 2010; Duan & Martín 2011) indicated that the Walz relation is valid only in CTBLs under adiabatic and quasi-adiabatic walls. In order to investigate the performance of the Walz relation in HLBLs, numerical simulation will be carried out next. The Navier–Stokes equations are solved using the finite-difference-based CFD code ACANS developed by the authors. The reliability of ACANS has been verified by numerous numerical simulation studies (Mo *et al.* 2022, 2023). The boundary conditions for numerical simulation in this paper are shown in table 1, where the wall temperature ratio Θ is defined as the ratio of the wall temperature to the adiabatic wall temperature, and $\Theta < 1$ implies a cold wall. In table 1, the notation M6Θ0.16, for example, denotes $Ma_\infty = 6$ and $\Theta = 0.16$, where the subscript ∞ denotes the freestream. The computational domain is 1 m in the streamwise direction and 0.5 m in the normal direction, with a
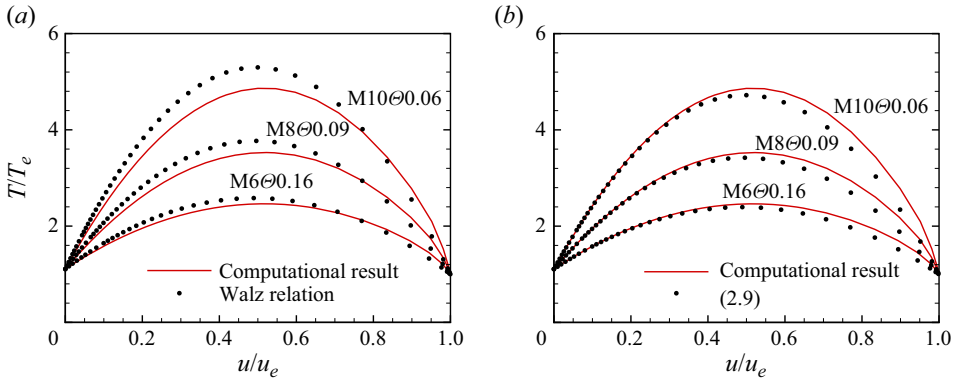
Figure 1. Comparisons of computational results with (*a*) Walz relation (2.1) and (*b*) (2.9).

two-dimensional orthogonal structured mesh, and the near-wall grids are encrypted to $\Delta y_1 = 10^{-6}$ m to achieve grid independence.

Figure 1(*a*) provides the comparison between computational results and the Walz relation for the cases M6Θ0.16, M8Θ0.09 and M10Θ0.06. It can be seen that the Walz relation fails under the severe cold wall effect, and the deviation is more obvious as the cold wall effect enhances. To overcome this problem, Zhang *et al.* (2014) proposed a new mean temperature–velocity relation for CTBLs by introducing the general recovery factor concept to consider the cold wall effect. However, this relation is derived by assuming the effective turbulent Prandtl number to be unity, and cannot be extended directly to laminar boundary layers. Therefore, it is necessary to conduct a derivation for HLBLs. Inspired by the work of Zhang *et al.* (2014), this paper similarly introduces the general recovery factor into HLBLs and assumes

$$H_g - H_w = \frac{Pr \, q_w}{\tau_w} u, \tag{2.2}$$

where $H_g = c_p T + r_g u^2/2$ is the general recovery enthalpy. However, unlike the derivation by Zhang *et al.* (2014), we differentiated (2.2) directly and obtained

$$r_g u + \frac{u^2}{2} \frac{\mathrm{d}r_g}{\mathrm{d}u} = c_p \left(\left.\frac{\mathrm{d}T}{\mathrm{d}u}\right|_w - \frac{\mathrm{d}T}{\mathrm{d}u} \right), \tag{2.3}$$

which could be rewritten as

$$T - \frac{u}{2} \left(\left.\frac{\mathrm{d}T}{\mathrm{d}u}\right|_w + \frac{\mathrm{d}T}{\mathrm{d}u} \right) = T_w + \frac{u^3}{4c_p} \frac{\mathrm{d}r_g}{\mathrm{d}u}. \tag{2.4}$$

Equation (2.4) exhibits a form different to the Zhang *et al.* (2014) derivation. To simplify this complex equation, we have investigated the distribution patterns of r_g in HLBLs, where r_g is calculated from the CFD results according to (2.2). Figure 2 illustrates the distributions of r_g in boundary layers of M6Θ0.16, M8Θ0.09 and M10Θ0.06, and the value of the original recovery factor r is employed as a reference. It can be found that r_g keeps constant throughout the boundary layer and smaller than r under all three conditions. Therefore, based on the conclusion that r_g is approximately constant,
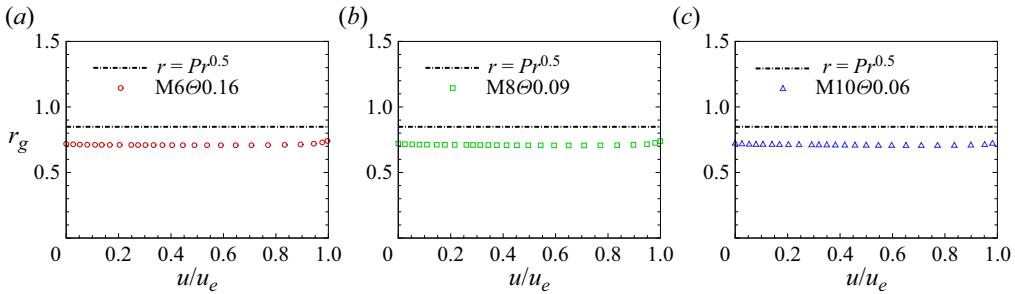
981 A9-4

Figure 2. Comparison between r_g and r in laminar boundary layers of (*a*) M6Θ0.16, (*b*) M8Θ0.09 and (*c*) M10Θ0.06.

we assume

$$\frac{\mathrm{d}r_g}{\mathrm{d}u} = 0, \tag{2.5}$$

thus (2.4) could be simplified to

$$T - \frac{u}{2}\left(\left.\frac{\mathrm{d}T}{\mathrm{d}u}\right|_w + \frac{\mathrm{d}T}{\mathrm{d}u}\right) = T_w. \tag{2.6}$$

Equation (2.6) is a first-order linear non-homogeneous ordinary differential equation, which naturally satisfies the wall boundary condition $u = 0, T = T_w$. Then this differential equation can be solved under the outer boundary conditions $u = u_e$, $T = T_e$, and the solution is

$$T = T_w + \left(u_e \left.\frac{\mathrm{d}T}{\mathrm{d}u}\right|_w\right)\frac{u}{u_e} + \left(T_e - T_w - u_e \left.\frac{\mathrm{d}T}{\mathrm{d}u}\right|_w\right)\left(\frac{u}{u_e}\right)^2. \tag{2.7}$$

Taking the derivative of (2.7) with respect to u, and combining with (2.3), we obtain

$$r_g = \frac{T_w - T_e}{u_e^2/(2c_p)} + \frac{2\,Pr}{u_e}\frac{q_w}{\tau_w}. \tag{2.8}$$

This equation yields the formula for calculating the general recovery factor under different flow conditions, which includes q_w and τ_w in addition to the boundary layer edge quantities and wall temperature. After that, employing the definition of the general total temperature $T_{rg} = T_e + r_g u_e^2/(2c_p)$, (2.7) can be rewritten as

$$T = T_w + (T_{rg} - T_w)\frac{u}{u_e} + (T_e - T_{rg})\left(\frac{u}{u_e}\right)^2. \tag{2.9}$$

It can be found that (2.9) and the Walz relation (2.1) are in similar form, with the difference that (2.9) introduces r_g to involve the $Pr \neq 1$ and cold wall effects simultaneously. For an adiabatic wall, r_g reduces naturally to r, and (2.9) degenerates to the Walz relation.

Figure 1(*b*) compares (2.9) with computational results for the cases M6Θ0.16, M8Θ0.09 and M10Θ0.06. It can be found that the temperature–velocity relation predicted by (2.9) collapses well with CFD results except for the region near the boundary layer edge, which shows a great improvement over the Walz relation. The above results indicate that (2.9) proposed in this paper can describe accurately the temperature–velocity relation in the laminar boundary layers with different compressibility and cold wall effects.

2.2. *Velocity law of the wall*

The theoretical basis of the velocity law of the wall in the viscous sublayer of CTBLs is the constant shear stress assumption (Gatski & Bonnet 2009), which assumes that the mean viscous shear stress τ_{xy} near the wall remains essentially unchanged along the wall-normal direction, and approximately equal to the wall shear stress τ_w (where the subscript w represents the wall surface), i.e. $\tau_{xy} \approx \mu \, \mathrm{d}u/\mathrm{d}y \approx \tau_w$, where μ is the dynamic viscosity. Then is there a region with constant shear stress near the wall in HLBLs?

Here, the order-of-magnitude analysis is performed for the zero-pressure gradient compressible flat-plate laminar boundary layer equations. The dimensionless continuity equation and the x-direction momentum equation can be expressed as

$$\begin{cases} \dfrac{\partial \rho^* u^*}{\partial x^*} + \dfrac{\partial \rho^* v^*}{\partial y^*} = 0, \\ \rho^* u^* \dfrac{\partial u^*}{\partial x^*} + \rho^* v^* \dfrac{\partial u^*}{\partial y^*} = \dfrac{1}{Re_\infty} \dfrac{\partial}{\partial y^*} \left(\mu^* \dfrac{\partial u^*}{\partial y^*} \right), \end{cases} \tag{2.10}$$

where superscript $*$ represents a dimensionless quantity, and $Re_\infty = \rho_\infty u_\infty L / \mu_\infty$, where L means the characteristic length of the flat plate. Here, we consider a certain thickness δ^- near the wall, with $\delta^- \ll \delta \ll L$, where δ is the boundary layer thickness. Obviously, there are $u^* \ll 1$, $x^* = O(1)$, $\mu^* = O(1)$, $y = O(\delta^-/L)$ within δ^-. Therefore, analysing the order of magnitude of the continuity equation yields $v^*/u^* = O(\delta^-/L)$. Further analysis of the order of magnitude of the momentum equation shows that the left-hand side yields $O(\rho^* u^{*2})$, and right-hand side yields $O(u^*/Re_\infty(\delta^-/L)^2)$. Therefore, when a certain thickness δ^- near the wall is small enough that $(\delta^-/L)^2 \leqslant 1/Re_\infty$, the ratio of the magnitudes of the left- and right-hand sides of the momentum equation is

$$\frac{\rho^* u^{*2}}{u^*} Re_\infty \left(\frac{\delta^-}{L} \right)^2 < 1 \times u^* Re_\infty \left(\frac{\delta^-}{L} \right)^2 \ll 1. \tag{2.11}$$

This indicates that the convective term in the x-direction momentum equation is sufficiently small compared to the viscous term and can be neglected within δ^-. Therefore, the momentum equation can be simplified to $\mu \, \mathrm{d}u/\mathrm{d}y \approx \tau_w$.

The above order of magnitude analysis proves that there is a 'constant shear stress layer' in compressible laminar flat-plate boundary layers near the wall, which has also been observed in the inner layer of CTBLs (Van Driest 2003; Griffin, Fu & Moin 2021, 2023; Bai, Griffin & Fu 2022) . Next, numerical simulations for HLBLs will be carried out to verify the above conclusion. Figure 3 shows the distribution of shear stress τ_{xy} in the boundary layers of M6Θ0.16, M8Θ0.09 and M10Θ0.06. It can be seen that for all cases, τ_{xy} remains essentially unchanged within $y/\delta < 0.1$, i.e. $\tau_{xy} \approx \tau_w$. This indicates that there is indeed a 'constant shear stress layer' near the wall of HLBLs.

Here, if we define the general friction velocity $u_\tau = \sqrt{\tau_w/\rho_w}$, then, according to the constant shear stress assumption, we obtain

$$\mathrm{d}y^* = \frac{\mu}{\mu_w} \, \mathrm{d}u^* \quad \text{or} \quad y^* = \int_0^{u^*} \frac{\mu}{\mu_w} \, \mathrm{d}u^* = U^*, \tag{2.12}$$

where $y^* = \rho_w u_\tau y / \mu_w$ and $u^* = u/u_\tau$ (to distinguish from y^+ and u^+ used in CTBLs). This velocity transformation is similar to that in CTBLs (Gatski & Bonnet 2009). Since the viscosity varies with temperature, the near-wall theoretical solution $y^* = u^*$ is obtained directly as the temperature remains basically constant near the wall (incompressible flows
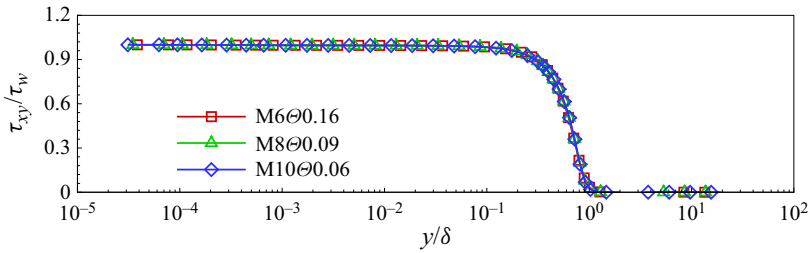
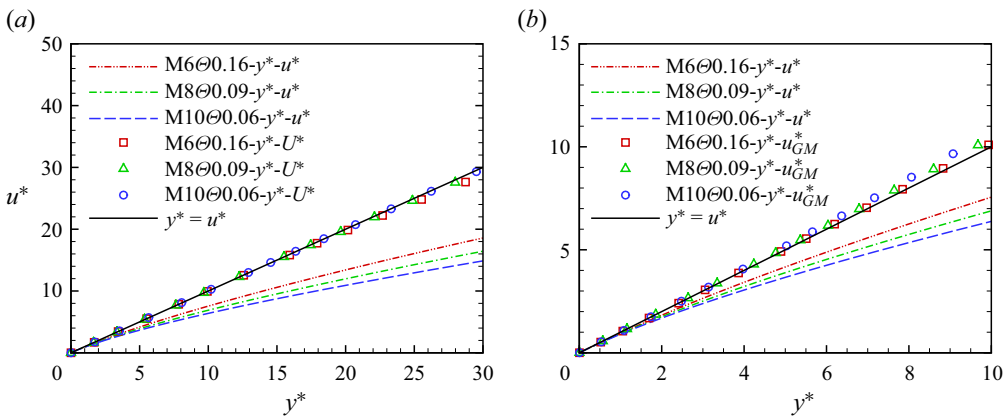Figure 3. Shear stress τ_{xy} in boundary layers of M6Θ0.16, M8Θ0.09 and M10Θ0.06.

Figure 4. Distributions of $y^* - u^*$, $y^* - U^*$ and $y^* - u_{GM}^*$ in HLBLs.

or adiabatic wall). However, for a cold wall boundary condition, the temperature changes sharply near the wall, and the variation of the viscosity should be considered. Here, the right-hand side of (2.12), which involves the viscosity variation, is denoted as U^*. The distributions of $y^* - u^*$ and $y^* - U^*$ in HLBLs are given in figure 4(*a*), and the incompressible theoretical solution $y^* = u^*$ is employed as a reference. It can be seen that $y^* - u^*$ deviates significantly from $y^* = u^*$ due to the cold wall effect, and the deviation becomes more obvious as the cold wall effect enhances and the Mach number increases. Here, $y^* - U^*$, which involves the cold wall effect, collapses well with $y^* = u^*$ in the range $y^* < 20$ ($y/\delta < 0.2$), indicating that (2.12) achieves a universal scaling for the velocity near the wall of the laminar boundary layers under different compressibility and cold wall effects.

However, it is not possible to use the integral form of (2.12) directly to construct the wall function. Therefore, the analytic velocity law of the wall will be derived next by using the new temperature–velocity relation. For air, the viscosity can be approximated by using the power law $\mu/\mu_w = (T/T_w)^{\omega}$. Then the temperature–velocity relation (2.9) is introduced, and (2.12) can be rewritten as

$$y^* = \int_0^{u^*} \left[1 + \frac{T_{rg} - T_w}{T_w} \frac{u}{u_e} + \frac{T_e - T_{rg}}{T_w} \left(\frac{u}{u_e} \right)^2 \right]^{\omega} \mathrm{d}u^*. \qquad (2.13)$$

To transform the integral form (2.13) into an analytic one, the above integrand is subjected to Taylor expansion, assuming that u/u_e is small in the near-wall region, and the small

quantities of second and higher order are ignored. After integration, we obtain

$$y^* = u^* \left[1 + \omega \frac{T_{rg} - T_w}{2T_w} \frac{u}{u_e} + \omega \frac{T_e - T_{rg}}{3T_w} \left(\frac{u}{u_e} \right)^2 \right] = u_{GM}^*. \tag{2.14}$$

Equation (2.14) is the analytic form of the near-wall velocity law of the wall proposed in this paper. It can be observed from (2.14) that the terms in the brackets, except for unity, relate to the cold wall effect. Therefore, the right-hand side of (2.14), which involves the cold wall effect, is denoted as u_{GM}^*. Then there is a linear form $y^* = u_{GM}^*$ similar to the incompressible one.

Figure 4(*b*) shows the distributions of $y^* - u_{GM}^*$ in HLBLs, and $y^* = u^*$ is employed as a reference. Comparing figure 4(*b*) with figure 4(*a*), it can be observed that $y^* - u_{GM}^*$ still collapses very well with $y^* = u^*$ within the range $y^* < 5$ ($y < 0.05\delta$), while the error occurs gradually as y^* increases (the error is introduced mainly by Taylor expansion), but the relative error remains less than 7 % in the range $y^* < 10$. Therefore, it can be concluded that (2.14) is valid near the wall.

3. Design and application of wall function method for laminar boundary layers

To design the new wall function method for HLBLs, numerical simulations are first conducted to analyse the variation pattern of the near-wall velocity and temperature with the change of Δy_1. Then the theoretical form of the new wall function and methodology of coupling with CFD results are designed based on the laws of the wall derived above. Finally, the new wall function method is applied to the simulation of typical HLBL flows to assess its effectiveness.

3.1. *Analysis of grid dependence of near-wall velocity and temperature*

Two numerical cases are designed to analyse the grid dependence of near-wall velocity and temperature in HLBLs over the flat plate. The dense mesh ($\Delta y_1 = 10^{-6}$) is used for the benchmark case, while the coarse one ($\Delta y_1 = 10^{-3}$) is employed for the comparative case. The freestream conditions of M8Θ0.09 in § 2.1 are adopted here, and the case of dense mesh is noted as DM8Θ0.09, while the other is CM8Θ0.09.

Figure 5 presents the velocity and temperature profiles in the boundary layers of DM8Θ0.09 and CM8Θ0.09 at the same downstream position. It can be observed that the velocity and temperature obtained from the coarse mesh almost coincide with the results from the dense mesh at the corresponding height. However, the coarse mesh cannot capture accurately the near-wall velocity and temperature gradient due to the insufficient grid resolution. At $x = 0.8$ m (position A), the errors of c_f and q_w are 18.5 % and 24.2 %, respectively (as shown in figure 6). Therefore, the key to reducing the grid dependence of c_f and q_w is to provide a method to calculate the c_f and q_w independent of Δy_1.

3.2. *Design of a new wall function method for HLBLs*

In the numerical simulation of CTBLs, the velocity and temperature at the first grid off the wall are deviated significantly from the accurate values when Δy_1 is enlarged, so the wall function must be coupled with CFD as a boundary condition to correct the velocity and temperature at the first grid. However, for HLBLs, the above simulations show that the velocity and temperature at the first grid off the wall are still accurate after Δy_1 is enlarged
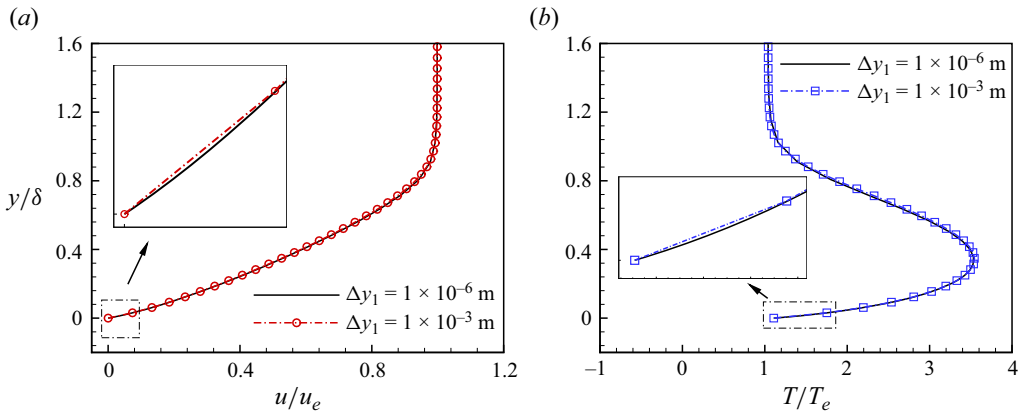
Figure 5. Comparisons between DM8Θ0.09 and CM8Θ0.09: (*a*) velocity profiles; (*b*) temperature profiles.
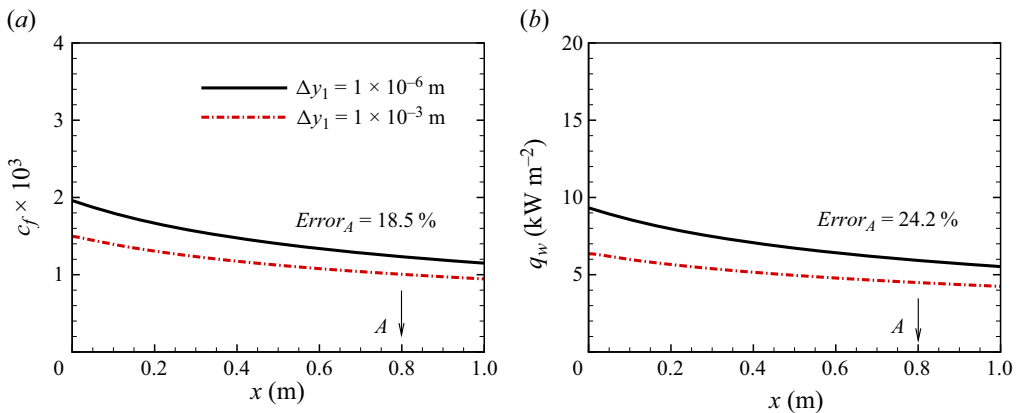

Figure 6. Comparisons of (*a*) c_f and (*b*) q_w between DM8Θ0.09 and CM8Θ0.09.

in a certain range. Therefore, the wall function method for HLBLs does not need to be involved in the iteration of CFD as a boundary condition, and there is only a requirement of designing a method to calculate c_f and q_w independent of Δy_1, that is, to perform post-processing after the simulation is completed.

Next, (2.9) and (2.14) are utilized to design post-processing methods for c_f and q_w to avoid the near-wall grid dependence. From (2.9) and (2.14), we can find that these equations contain multiple boundary layer edge quantities (such as u_e, T_e), which are difficult to obtain in simulations of practical complicated configurations. Therefore, the direct use of these equations to derive the wall function will inevitably introduce the boundary layer edge quantities, which will not facilitate the application of the wall function. To deal with this issue, a new prescription is proposed next. For the temperature–velocity relation, if the differential equation (2.6) is solved by supposing new outer boundary conditions $u = u_{e^-}$, $T = T_{e^-}$, where the subscript e^- denotes a reference point inside the boundary layer instead of the real boundary layer edge, then the following extended temperature–velocity relation can be obtained:

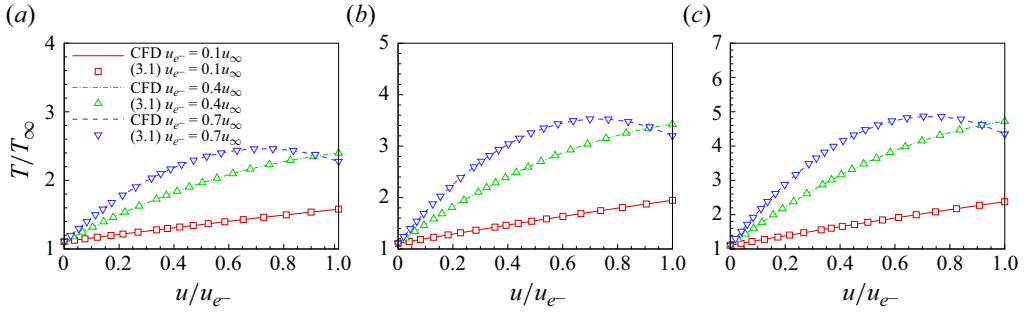$$T = T_w + (T_{rg} - T_w) \frac{u}{u_{e^-}} + (T_{e^-} - T_{rg}) \left(\frac{u}{u_{e^-}} \right)^2, \tag{3.1}$$

Figure 7. Comparisons between (3.1) and CFD results: (*a*) M6Θ0.16, (*b*) M8Θ0.09 and (*c*) M10Θ0.06.

where T_{rg} is similar to the definition in § 2.1, except that the quantities at the reference point are used to replace those at the boundary layer edge.

From (3.1), it can be found that the velocity–temperature relation does not have to relate to the boundary layer edge quantities, but requires only selecting a certain reference point e^- within the boundary layer. Figure 7 compares the temperature–velocity relation between (3.1) and CFD results in HLBLs of M6Θ0.16, M8Θ0.09 and M10Θ0.06. Here, (3.1) is calculated by selecting three typical positions within the HLBLs – $u_{e^-} = 0.1u_\infty$, $u_{e^-} = 0.4u_\infty$, and $u_{e^-} = 0.7u_\infty$ – as reference points, respectively. It can be seen that (3.1) collapses well with the CFD results, which indicates that it successfully avoids introducing the boundary layer edge quantities while still ensuring the accuracy of the results. Moreover, for the velocity law of the wall (2.14), it can be extended further as

$$y^* = u^* \left[1 + \omega \frac{T_{rg} - T_w}{2T_w} \frac{u}{u_{e^-}} + \omega \frac{T_{e^-} - T_{rg}}{3T_w} \left(\frac{u}{u_{e^-}} \right)^2 \right]. \tag{3.2}$$

Next, the laminar wall function is derived based on the extended laws of the wall. For convenience, the second grid point off the wall is taken as the reference point in the wall function, since the selection of the reference point is arbitrary in the wall-normal direction within the HLBLs. After reorganizing (3.1), q_w can be written directly as

$$q_w = \frac{T_1 - T_w + (T_w - T_2)(u_1/u_2)^2}{Pr\,(u_1^2/u_2 - u_1)} c_p \tau_w. \tag{3.3}$$

The union of (3.1) and (3.2) yields immediately

$$\tau_w = \frac{u_1 \mu_w}{\Delta y_1} \left[1 + \frac{\omega}{T_w u_2} \left(\frac{2u_1 - 3u_2}{6} \right) \frac{T_1 - T_w + (T_w - T_2)(u_1/u_2)^2}{u_1/u_2 - 1} \right.$$
$$\left. - \omega \frac{T_w - T_2}{3T_w} \left(\frac{u_1}{u_2} \right)^2 \right]. \tag{3.4}$$

Equations (3.3) and (3.4) are the theoretical forms of the laminar wall function proposed in this paper, and the subscripts 1 and 2 on the right-hand side denote the quantities at the first and second grid points off the wall, respectively. In this way, the power law could be used to provide an accurate $\omega = \ln(\mu_1/\mu_w)/\ln(T_1/T_w)$. Therefore, the laminar wall function can calculate directly c_f and q_w based on the values at the wall as well as the values at the first and second grid points off the wall.
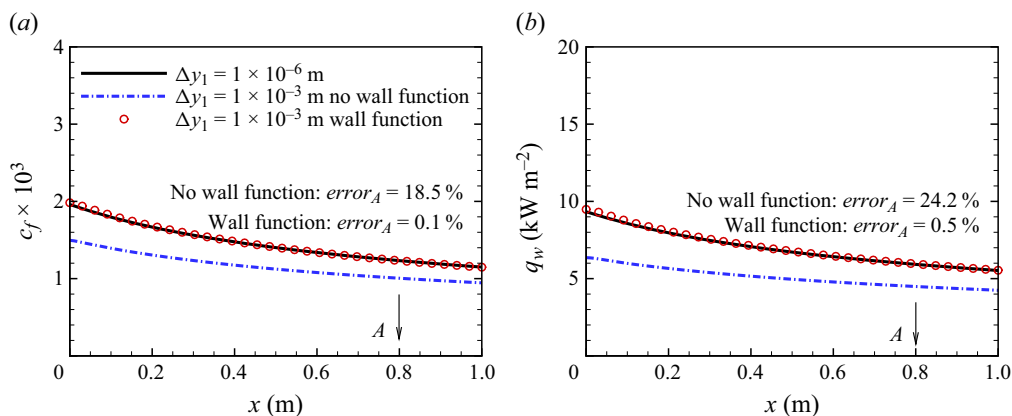
981 A9-10

Figure 8. Comparisons of (*a*) c_f and (*b*) q_w between DM8Θ0.09 and CM8Θ0.09.

3.3. *Applications of the new wall function method for HLBLs*

Next, this subsection will conduct research on the applications of the laminar wall function for typical HLBL flows. On the one hand, the effectiveness of the laminar wall function method will be verified, and on the other hand, the maximum relaxation degree of Δy_1, while ensuring the accuracy of the results of the laminar wall function, will be investigated.

3.3.1. *Hypersonic flows over the flat plate*

The first application of the new wall function method is carried out based on the CM8Θ0.09 case, which simulates an HLBL over a flat plate. Here, τ_w and q_w are calculated by the laminar wall function proposed in § 3.2. It can be seen from figure 8 that the CFD results using the laminar wall function collapse well with the exact results, and the errors of c_f and q_w at $x = 0.8$ m (point *A*) are only 0.1 % and 0.5 %, respectively, indicating that the new wall function proposed in this paper can reduce effectively the grid dependence (Δy_1) of c_f and q_w.

For computational efficiency, figure 9 compares the residuals of the CM8Θ0.09 and DM8Θ0.09 cases under the same Courant–Friedrichs–Lewy (CFL) condition, CFL = 0.4. Eventually, if the residuals drop by eight orders of magnitude is used as the convergence criterion, then the dense mesh needs to advance 5.5×10^5 steps, while the coarse one needs only 1.1×10^4 steps, and the efficiency is enhanced by 50 times. Obviously, the enlargement of Δy_1 relaxes the local time step, which accelerates the simulation convergence.

3.3.2. *Hypersonic flows over the curved walls*

The second application of the new wall function method is carried out based on the HLBL flows over the curved walls. A schematic diagram of the two-dimensional curved wall used in the numerical simulation is shown in figure 10. This configuration contains two parts: the first part is a flat plate with streamwise length $L_1 = 1$ m, while the second part is a curved wall connected smoothly to the first one with a specific constant curvature radius ϱ. This curved wall shapes a circumference angle $\theta = 10°$, and streamwise length $L_2 = 1$ m. In this subsubsection, two different types of curved walls will be employed, with curvature radii 5.76 m and -5.76 m, respectively. Obviously, the HLBLs undergo
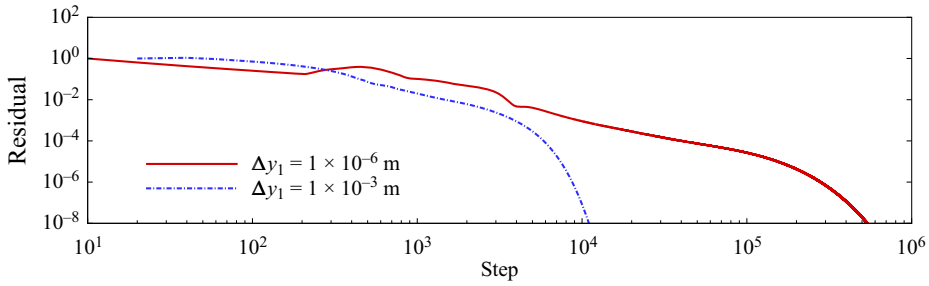
Figure 9. Comparison of residuals between DM8Θ0.09 and CM8Θ0.09.

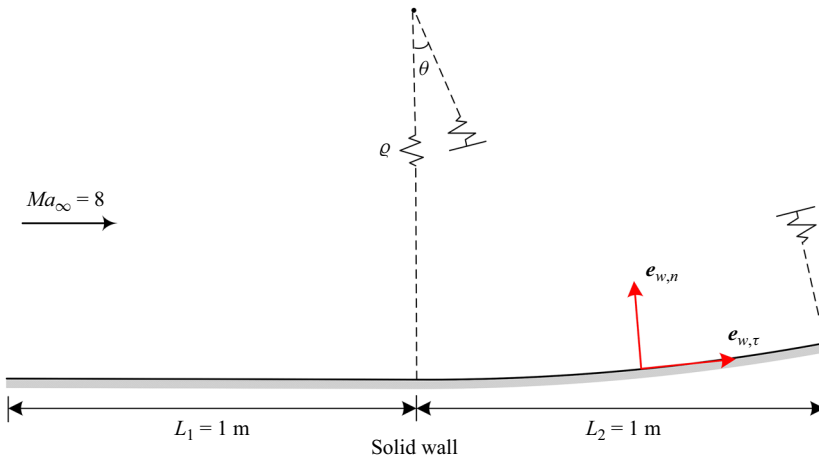Figure 10. A schematic diagram of the two-dimensional curved wall.

compression through the 'upward' curved wall with positive ϱ, while expansion through the 'downward' curved wall with negative ϱ.

Figure 11 first illustrates the velocity and density contours of Mach 8 hypersonic flows over the two different types of curved walls. As we can see, beyond the boundary layer, the flow quantities of the mainstream are changing along the streamwise direction due to the compression or the expansion caused by the curved walls. In other words, the position of the boundary layer edge and the corresponding flow quantities will be difficult to determine. Therefore, it is essential to avoid introducing boundary layer edge quantities when applying the laminar wall function method to such flows, and the concept of a 'reference point' proposed in § 3.2 is precisely to deal with this issue.

However, if the wall function designed in § 3.2 is extended to HLBLs over the curved walls, then it is important to note that

$$U_j = V_j \cdot e_{w,\tau}, \tag{3.5}$$

which is the local velocity vector V_j projected onto the tangential direction of the wall surface, should be used rather than the local streamwise velocity u_j, where j represents the jth grid over the wall, and $e_{w,\tau}$ denotes the unit tangent vector of the wall.

Here, the cases of positive ϱ will be studied first. Due to the flow convergence caused by the 'upward' curved wall, the boundary layer thickness in the downstream part is thinner than the upstream one. Therefore, the coarse mesh with $\Delta y_1 = 5 \times 10^{-4}$ m was
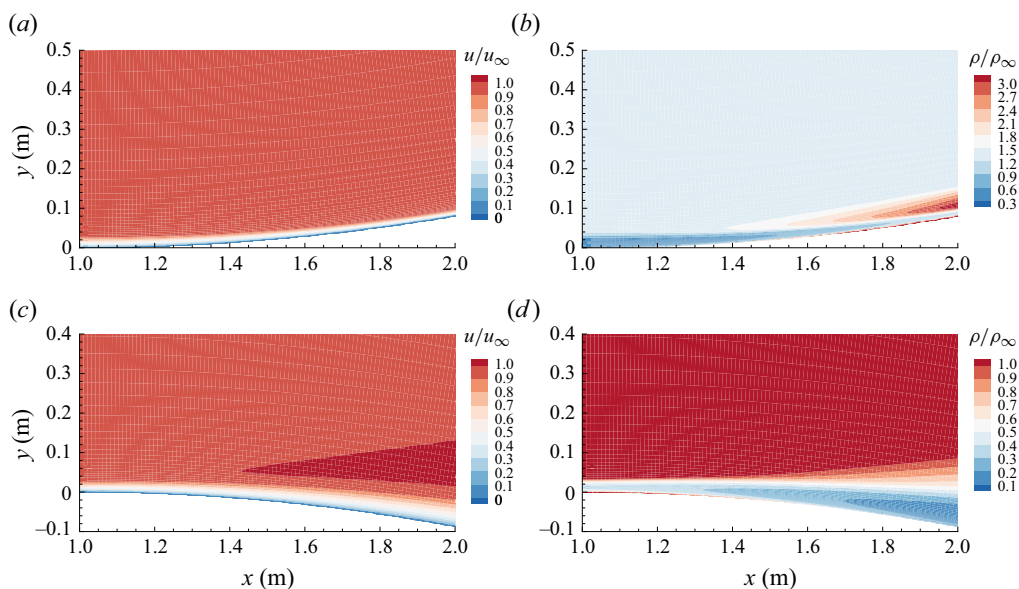
981 A9-12

Figure 11. Velocity and density contours of Mach 8 hypersonic flows over the curved walls.

selected, while the dense mesh is consistent with the previous study with $\Delta y_1 = 10^{-6}$ m. It should be noted that Δy_1 represents the distance from the wall to the first grid rather than the difference in the y-coordinate. Figures 12(a,b) show the comparisons of c_f and q_w, respectively, between the dense mesh and the coarse mesh. It can be seen that the simulation results in the upstream part are similar to those in § 3.3.1; however, the c_f and q_w predicted by the dense mesh in the downstream part are increased gradually along the streamwise direction, which is due to the significant thinning of the boundary layer along the streamwise direction. Although the results of the coarse mesh without using wall functions also increase along the streamwise direction, the error increases gradually compared to the dense mesh. Fortunately, the laminar wall function method proposed in this paper predicts that the results agree well with those for the dense mesh; at $x = 1.6$ m, the errors of c_f and q_w are 1.7 % and 1.9 %, respectively.

Next, the cases of negative ϱ have also been investigated. Due to the flow divergence caused by the 'downward' curved wall, the boundary layer thickness in the downstream part is thicker than in the upstream part. Therefore, Δy_1 of the coarse and the dense mesh are consistent with the previous studies. Figures 13(a,b) show the comparisons of c_f and q_w, respectively, between the dense mesh and the coarse mesh. It can be seen that the simulation results in the upstream part are consistent with those in § 3.3.1; however, c_f and q_w decrease rapidly in the downstream part, which is due to the significant thickening of the boundary layer along the streamwise direction. Although the results of the coarse mesh without using wall functions also decrease along the streamwise direction, the errors of c_f and q_w at $x = 1.6$ m are still 13.1 % and 17.4 %, respectively. However, the laminar wall function method proposed in this paper still predicts that the results agree well with those for the dense mesh; at $x = 1.6$ m, the errors of c_f and q_w are 1.7 % and 1.9 %, respectively.

The above results indicate that the new wall function method can still effectively reduce the near-wall grid dependence of the simulation results for HLBL flows over the more complex curved walls. In fact, the new wall function can provide accurate c_f and q_w as
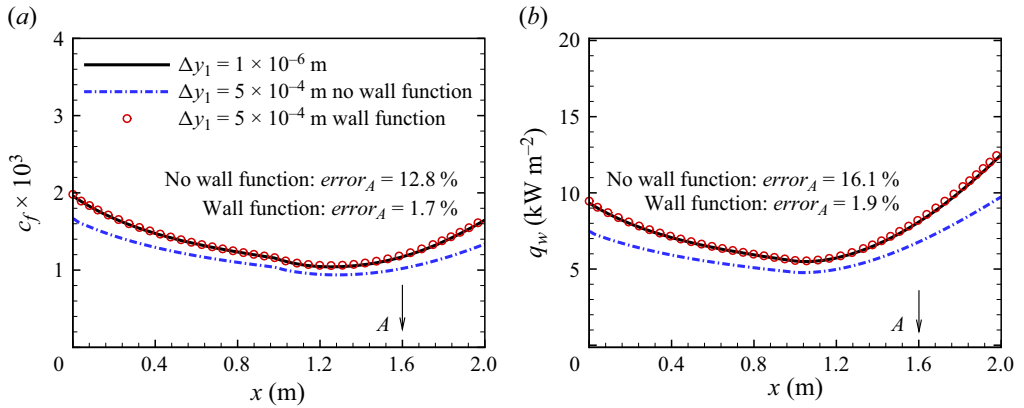
Figure 12. Comparisons of (*a*) c_f and (*b*) q_w among the dense mesh, the coarse mesh with wall function, and the coarse mesh without wall function.
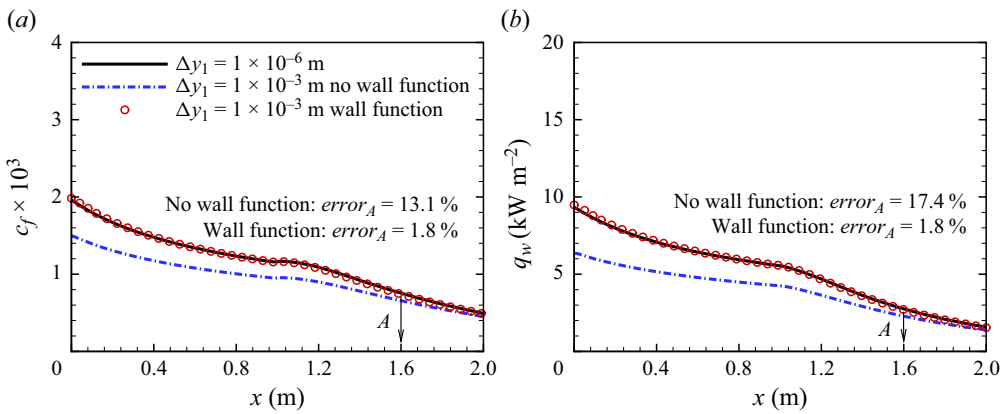

Figure 13. Comparisons of (*a*) c_f and (*b*) q_w among the dense mesh, the coarse mesh with wall function, and the coarse mesh without wall function.
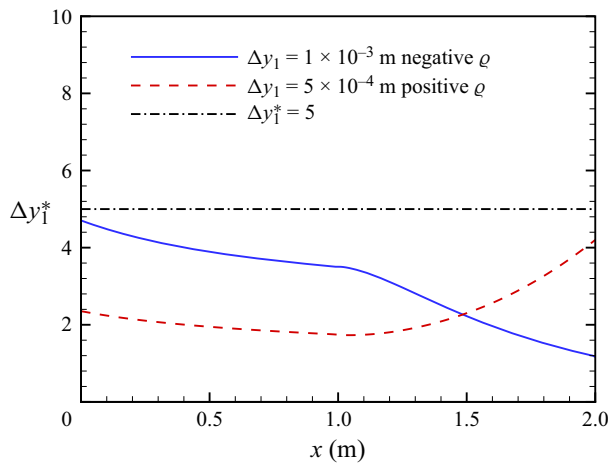

Figure 14. Distributions of Δy_1^* along the streamwise direction. Blue solid line indicates the coarse mesh of curved wall with positive ϱ; red dashed line indicates the coarse mesh of curved wall with negative ϱ; black dash-dotted line indicates constant $\Delta y_1^* = 5$ for reference.

long as the mesh satisfies $\Delta y_1^* < 5$. Figure 14 presents the distribution of Δy_1^* along the streamwise direction, with a blue solid line denoting the coarse mesh of the 'upward' curved wall, and a red dashed line representing the coarse mesh of the 'downward' curved wall. As we can see, the maximum value of Δy_1^* appears at $x = 0$ m in the case of negative ϱ shape, while at $x = 2$ m in the case of positive ϱ shape, it is worth noting that Δy_1^* of two cases remains less than 5 throughout the entire simulation domain. From another perspective, in figure 4(*b*), the error caused by Taylor expansion in the analytic velocity law of the wall basically can be ignored as long as $\Delta y_1^* < 5$. However, this error increases gradually and reaches 7 % when $\Delta y_1^* = 10$, which will deteriorate the wall function results directly. Therefore, it can be concluded that the new wall function method can reduce Δy_1 significantly in the simulation of HLBL flows while keeping $\Delta y_1^* < 5$ to acquire precise results.

4. Conclusions

In this paper, a new wall function method is proposed for hypersonic laminar boundary layers (HLBLs) to reduce the near-wall grid dependence of c_f and q_w in numerical simulations, aiming for fast and accurate predictions. First, the near-wall 'constant shear stress layer' is verified in HLBLs through numerical simulation, and an analytic laminar velocity law of the wall is derived based on this truth, which achieves a universal scaling of the near-wall velocity of HLBLs under different compressibility and cold wall effects. Then a more accurate temperature–velocity relation is derived theoretically by introducing the general recovery factor concept in compressible turbulent boundary layers (CTBLs) to address the invalidation of the Walz relation in HLBLs under the cold wall effect.

Based on the above laminar laws of the wall, a new wall function method for HLBLs is proposed. In order to avoid introducing the boundary layer edge quantities that make it difficult to apply the wall function in the simulation of complicated configurations, the extended laminar laws of the wall are derived theoretically by modifying the outer boundary conditions of the differential equation in deriving the temperature–velocity relation. Moreover, unlike the wall function method used in CTBLs, the new wall function obtains directly the accurate c_f and q_w by simply post-processing without being involved in the iteration of simulation. The numerical experiments of Mach 8 HLBLs over the flat plate show that effectively, the new wall function can enlarge the distance Δy_1 of the first grid point off the wall from 10^{-6} m to 10^{-3} m, and the simulation errors of c_f and q_w of the mesh with $\Delta y_1 = 10^{-3}$ m are reduced significantly, from 24.2 % and 18.5 % to 0.5 % and 0.1 %, respectively. This relaxes the restrictions on the integration time step, and a 50 times enhancement of the simulation efficiency is achieved. Due to the new wall function removing the boundary layer edge quantities, success is also achieved under the curved walls. Additionally, further analysis indicates that it is necessary to keep the non-dimensional $\Delta y_1^* < 5$ in the simulation of HLBL flows to ensure the precision of the new wall function.

Declaration of interests. The authors report no conflict of interest.

Author ORCIDs.

🆔 Fan Mo https://orcid.org/0000-0003-2037-6489;

🆔 Zhenxun Gao https://orcid.org/0000-0002-0130-0334.

REFERENCES

ANDERSON, J. 2006 *Hypersonic and High Temperature Gas Dynamics*, 2nd edn. McGraw-Hill.

BAI, T., GRIFFIN, K. & FU, L. 2022 Compressible velocity transformations for various noncanonical wall-bounded turbulent flows. *AIAA J.* **60** (7), 4325–4337.

DUAN, L., BEEKMAN, I. & MARTÍN, M. 2010 Direct numerical simulation of hypersonic turbulent boundary layers. Part 2. Effect of wall temperature. *J. Fluid Mech.* **655**, 419–445.

DUAN, L. & MARTÍN, M. 2011 Direct numerical simulation of hypersonic turbulent boundary layers. Part 4. Effect of high enthalpy. *J. Fluid Mech.* **684**, 25–59.

GAO, Z., JIANG, C. & LEE, C. 2013 Improvement and application of wall function boundary condition for high-speed compressible flows. *Sci. China* **56**, 2501–2515.

GATSKI, T. & BONNET, J. 2009 *Compressibility, Turbulence and High Speed Flow*. Elsevier.

GRIFFIN, K., FU, L. & MOIN, P. 2021 Velocity transformation for compressible wall-bounded turbulent flows with and without heat transfer. *Proc. Natl Acad. Sci. USA* **118** (34).

GRIFFIN, K., FU, L. & MOIN, P. 2023 Near-wall model for compressible turbulent boundary layers based on an inverse velocity transformation. *J. Fluid Mech.* **970**, A36.

HOFFMANN, K., SIDDIQUI, M. & CHIANG, S. 2013 Difficulties associated with the heat flux computations of high speed flows by the Navier–Stokes equations. In *Aerospace Sciences Meeting*. AIAA.

MO, F., LI, Q., ZHANG, L. & GAO, Z. 2023 Direct numerical simulation of hypersonic wall-bounded turbulent flows: an improved inflow boundary condition and applications. *Phys. Fluids* **35**, 035135.

MO, F., SU, W., GAO, Z., DU, C., JIANG, C. & LEE, C. 2022 Numerical investigations of the slot blowing technique on the hypersonic vehicle for drag reduction. *Aerosp. Sci. Technol.* **121**, 107372.

NICHOLS, R. & NELSON, C. 2004 Wall function boundary conditions including heat transfer and compressibility. *AIAA J.* **42** (6), 1107–1114.

THIVET, F., BESBES, O. & KNIGHT, D. 2013 Effect of grid resolution on accuracy of skin friction and heat transfer in turbulent boundary layers. In *Aerospace Sciences Meeting and Exhibit*. AIAA.

VAN DRIEST, E.R. 2003 Turbulent boundary layer in compressible fluids. *J. Spacecr. Rockets* **40** (6), 1012–1028.

WALZ, A. 1969 *Boundary Layers of Flow and Temperature*. MIT.

WHITE, F. 1991 *Viscous Fluid Flow*. Osborne McGraw-Hill.

WILCOX, D. 2006 *Turbulence Modeling for CFD*. DCW Industries.

ZHANG, Y., BI, W., HUSSAIN, F. & SHE, Z. 2014 A generalized Reynolds analogy for compressible wall-bounded turbulent flows. *J. Fluid Mech.* **739**, 392–420.